

Quantum Fidelity of the Aubry-André Model and the Exponential Orthogonality Catastrophe

J. Vahedi*

Department of Physics and Earth Sciences, Jacobs University Bremen, Bremen 28759, Germany

S. Kettemann†

*Department of Physics and Earth Sciences, Jacobs University Bremen, Bremen 28759, Germany and
Division of Advanced Materials Science, Pohang University of
Science and Technology (POSTECH), Pohang 790-784, South Korea*

We consider the orthogonality catastrophe in the (extended) Aubry-André (AA)-Model, by calculating the overlap F between the ground state of the Fermi liquid in that quasi-crystalline model and the one of the same system with an added potential impurity, as function of the size of that impurity. Recently, the typical fidelity F_{typ} was found in quantum critical phases to decay exponentially with system size L as $F \sim \exp(-cL^{z\eta})$ ⁸ as found in an analytical derivation due to critical correlations. For the critical AA model $\eta = 1/2$ is the power of multifractal intensity correlations, and z the dynamical exponent due to the fractal structure of the density of states which is numerically found to be $z \gg 1$. Therefore, we aim here to check this prediction by numerical finite size scaling. Surprisingly, however, we find for a weak single site impurity that the fidelity decays with a power law, in the critical phase. Even though it is found to be smaller and decays faster than in the metallic phase, it does not decay exponentially as predicted. We find an exponential AOC however in the insulator phase for which we give a statistical explanation, a mechanism which is profoundly different from the AOC in metals, where it is the coupling to a continuum of states which yields there the power law suppression of the fidelity. By reexamination of the analytical derivation we identify nonperturbative corrections due to the impurity potential and multipoint correlations among wave functions as possible causes for the absence of the exponential AOC in the critical phase. For an extended impurity, however, we find indications of an exponential AOC at the quantum critical point of the AA model and at the mobility edge of the extended AA model and suggest an explanation for this finding. Furthermore we consider a parametric perturbation to the AA model, and find an exponential AOC numerically, in agreement with an analytical derivation which we provide here.

PACS numbers:

I. INTRODUCTION

The quantum fidelity F , the absolute value of the scalar product between the ground state of a quantum system $|\psi\rangle$ and the ground state after a perturba-

tion $|\psi'\rangle$, at fixed density of fermions $n = N/L^d$, $F = |\langle \psi | \psi' \rangle|$ is known to vanish with a power law of the system size L in a metallic phase, the celebrated Anderson orthogonality catastrophe.¹ Anderson showed in Ref.1 that the fidelity has a strict upper bound,

$$F = |\langle \psi | \psi' \rangle| < \exp(-I_A), \quad (1)$$

where the Anderson integral I_A is for noninteracting electrons given in terms of the single particle eigenstates of the original system $|n\rangle$ and the new system $|n'\rangle$ by

$$I_A = \frac{1}{2} \sum_{n=1}^N \sum_{n'>N} |\langle n | n' \rangle|^2. \quad (2)$$

If the added impurity is short ranged and of strength V_0 , Anderson found for a clean metal $I_A = (1/2)\rho_0^2 V_0^2 \ln N$, where ρ_0 is the density of states at the Fermi energy, diverging with the number of Fermions N , so that F decays with a power law with $N = nL^d$, the so called Anderson orthogonality catastrophe (AOC). According to Eq. (2) this suppression is a consequence of the fact that the local perturbation connects the Fermi liquid to a continuum of excited states. This has therefore important experimental consequences like the singularities in X-Ray absorption and emission of metals.² Furthermore, the zero bias

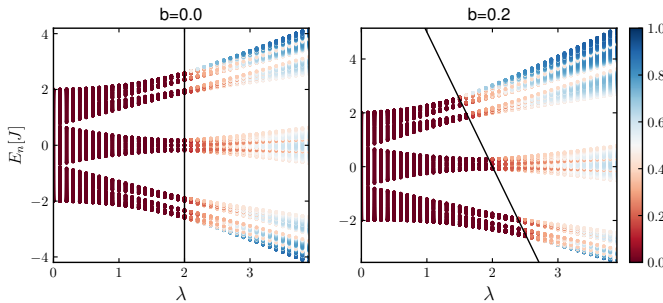


FIG. 1: Inverse participation ratio $\text{IPR} = \sum_i |\psi_i|^4$ as function of energy and parameter λ for the AA-model (left), and the EAA-model with $b = 0.2$ (right), where a mobility edge (black solid line) separates the extended phase $\text{IPR} \rightarrow 0$ from the localized $\text{IPR} \rightarrow a/\xi$, where ξ is the localization length and a the lattice spacing. System size is $L = 610$.

anomaly in disordered metals³ and anomalies in the tunneling density of states in quantum Hall systems⁴ are related to the OC. The concept of fidelity can be generalized to any parametric perturbation of a system and be used to characterize quantum phase transitions.⁵ A relationship between the orthogonality catastrophe and the adiabaticity breakdown in a driven many-body system has been shown in Ref.⁶ The orthogonality catastrophe can be studied in ensembles of ultracold atoms in a controlled way.⁷

Recently, it has been found that the AOC with a local impurity can be exponential at any quantum critical point, as obtained in an analytical derivation.⁸ There, the coupling to a continuum of excited states due to the impurity was found to be enhanced by quantum critical power law correlations. On the other hand, it has been argued in Refs.⁹ and⁸ that in an Anderson insulator the fidelity with a local impurity remains typically finite since the impurity can couple only to a discrete number of states. In Refs.^{10,11}, however, an exponential AOC was found numerically in Anderson-localized Fermi systems, when the perturbation is turned on adiabatically slowly.

In order to clarify the existence of an exponential AOC, here we aim to study the fidelity in the (extended) quasicrystalline Aubry-André-Model.^{12–14} The AA-model has a quantum phase transition from a metal to a localised phase as function of a parameter λ and a quantum critical point $\lambda = 2$, see Fig. 1 (left). In a recent study¹⁵ the AOC at the critical point of this model has been studied and found numerically to follow a power law. This is an another motivation for us, to reconsider the fidelity in this model and to examine whether the exponential AOC predicted in Ref.⁸ at a quantum critical point exists in the critical AA-Model. Moreover, this model and its extensions can be realised in ultracold atoms, allowing the tuning of parameters and perturbations in a controlled way.⁷

The (extended) Aubry-André-Model has the Hamiltonian,¹²¹⁴

$$H_{EAA} = -J \sum_{i=1}^L (c_i^\dagger c_{i+1} + c_{i+1}^\dagger c_i) + \lambda \sum_{i=1}^L \frac{\cos(2\pi Qi + \phi)}{1 - b \cos(2\pi Qi + \phi)} c_i^\dagger c_i, \quad (3)$$

where J is the hopping amplitude (we set $J = 1$ as the unit of energy), c_i^\dagger and c_i are creation and annihilation operators of a spinless fermion at site i on a chain of L sites, and λ presents the amplitude of the quasiperiodic potential. Q is an irrational number usually chosen to be the golden ratio, $Q = 2/(\sqrt{5} + 1)$, and ϕ is a randomly chosen phase interval $[0, 2\pi]$ that is the same for all sites. The open boundary conditions are considered throughout the results presented in the paper. The parameter b can take values $b \in [0, 1)$. For $b = 0$ we recover the Aubry-André-Model, which has no mobility edge in the energy

spectrum, but when the parameter λ is changed all states undergo a transition from localized $\lambda > 2$, critical $\lambda = 2$ to extended for $\lambda < 2$,¹² as seen in Fig. 1 (left), where the inverse participation ratio ($\text{IPR} = \sum_i |\psi_i|^4$) is plotted versus energy and parameter λ . At the critical point $\lambda_c = 2$, all eigenstates are known to be multifractal.¹³ Moreover the model has a fractal energy spectrum, where the level spacing Δ scales with system size L as z , $\Delta \sim L^{-z}$, where the dynamical exponent z can be different from the dimension of the model $d = 1$.

For $b \neq 0$ the EAA-model shows a mobility edge given by $E_{\text{mb}} = (2J - \lambda)/b$,¹⁴ as seen in Fig. 1 (right), where the inverse participation ration (IPR) is plotted as function of energy and parameter λ . The mobility edge (black solid line) separates the extended phase $\text{IPR} \rightarrow 0$ from the localized $\text{IPR} \rightarrow a/\xi$, where a is the lattice spacing and ξ the localization length.

The paper is organised as follows. In section II we review the definition of the ground state fidelity F in the presence of an impurity and its upper bound provided by the exponential of the Anderson integral. In section III we define the Anderson integral with an extended impurity. In section IV we review the spectrum of the AA model, and study how it is modified by an impurity. In section V we present all results for the fidelity of a single site impurity in the AA model. We begin with presenting the numerical results in section V. A. The analytical results in the approximation used in Ref.⁸ are reviewed and applied for the AA model with a single site impurity in section V. B yielding an exponential AOC in the critical phase. As this is in disagreement with the numerical results presented in section V. A, we consider corrections to the Anderson integral in section V. C beyond the approximation used in section V. B. We thereby succeed to identify a mechanism which yields a potential AOC in the critical phase, in agreement with the numerical results. In section V. D we show that in the insulator regime there is a statistical mechanism which yields an exponential AOC in agreement with the numerical results in the insulator phase of the AA model. In section VI we present results for the fidelity with an extended impurity, and provide evidence for an exponential AOC in the critical regime, when the impurity extends over more than one sites. By analysing the Anderson integral for an extended impurity we suggest a mechanism which explains this discovery of an exponential AOC in the critical phase. In section VII we present numerical results for the ground state fidelity with a parametric perturbation giving evidence for an exponential AOC. Analysing the Anderson integral for that perturbation we give a derivation which is in agreement with these numerical results. In section VIII we present numerical results for the ground state fidelity in the extended AA model. We conclude with section IX. In Appendix A we review the derivation of an upper bound for the ground state fidelity. In Appendix B we give details for the derivation of the AOC with a single site impurity. In Appendix C we present numerical benchmark results for the fidelity

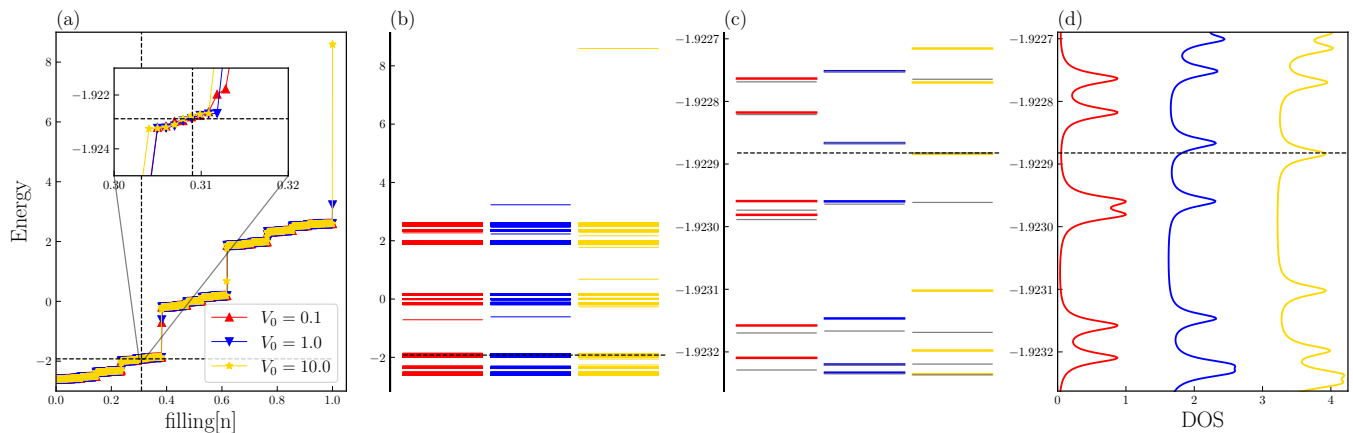


FIG. 2: (a) Energy spectrum at the critical point $\lambda = 2.0$ as function of filling n for a single impurity case. Results of three different impurity strength V_0 are displayed in colored symbols. The horizontal dashed line is the Fermi energy. Inset: zoomed energies close to the Fermi energy without the impurity $E_F/J = -1.922882$, corresponding to filling $n = 0.309$. (b) and (c) show the complete energy diagram, and a zoom close to the E_F , with and without (grey) impurity. (d) density of state (DOS) as function of energy close to E_F . The results are randomly chosen from one of the realizations. For calculating DOS broadening $\eta = 1e^{-5}$ is utilized. System size $L = 1024$.

of the 1D tight binding model with an impurity.

II. GROUND STATE FIDELITY

To derive the ground state fidelity we first diagonalise the Hamiltonian as given by Eq. (3). As the model is non interacting, it can be diagonalised with the basis change as. $H_{AA} = \sum_n \epsilon_n d_n^\dagger d_n$, with the one-electron energy Eigenvalues ϵ_n , and the creation and annihilation operators in the single particle Eigenstates $|n\rangle$ given by $d_n = \sum_i \psi_{ni} c_i$, where ψ_{ni} are complex coefficients. Then, the ground state can be constructed as $|\psi\rangle = \prod_{n=1}^N d_n^\dagger |0\rangle$, with fixed number of particles N and fixed particle filling $n = N/L$. When adding a perturbation the filling n remains fixed, while the Fermi energy can change.

Next, we introduce an impurity, which extends over a finite subset S_M of M neighboured lattice sites with $S_M = i, i+1, \dots, i+M-1$ with

$$H_{imp} = \frac{1}{M} V_0 \sum_{i \in S_M} c_i^\dagger c_i. \quad (4)$$

In the numerical implementation we choose the center of the impurity to be located at the lattice center $L/2$. The non interacting Hamiltonian perturbed by the impurity $H' = H_{AA} + H_{imp}$ has the new Eigenstates $|n'\rangle$, yielding $H' = \sum_{n'} \epsilon'_{n'} d_{n'}^\dagger d_{n'}$, where $d_{n'} = \sum_i \psi_{n'i} c_i$, with complex coefficients $\psi_{n'i}$. Thereby, the new ground state is given by $|\psi'\rangle = \prod_{n'=1}^N d_{n'}^\dagger |0\rangle$. Thus, the fidelity is given by $F = |\langle \psi' | \psi \rangle| = |\det(A)|$, where A is the $N \times N$ matrix where the matrix elements are the scalar products of the Eigenstates before and after the perturbation, $A_{nn'} = \langle n | n' \rangle$, see Appendix A for more details.

III. ANDERSON INTEGRAL

Before presenting the numerical results, let us first review the rigorous upper limit of the fidelity, as given by the right hand side of Eq. (1), whose derivation is given in Appendix A. The Anderson integral Eq. (2) can be rewritten for the impurity perturbation Eq. (4) without approximation as

$$\begin{aligned} I_A &= \frac{1}{2} \sum_{n=1}^N \sum_{n' > N} \frac{1}{(E_{n'} - E_n)^2} |\langle n | H_{imp} | n' \rangle|^2 \\ &= \frac{V_0^2}{2M^2} \sum_{n=1}^N \sum_{n' > N} \frac{|\sum_{i \in S_M} \psi_{ni}^* \psi_{n'i}|^2}{(E_{n'} - E_n)^2}, \end{aligned} \quad (5)$$

where $\psi_{ni} = \langle n | i \rangle$, $\psi_{n'i} = \langle n' | i \rangle$, is the local amplitude with and without the additional impurity at site i . Eq. (5) can be rewritten by replacing the summation over energy Eigenvalues $E_{n'}, E_n$ by an integral over energy with density of states $\rho(E)$ without the impurity, and $\rho'(E')$ with the impurity. Thus, we get

$$\begin{aligned} I_A &= \frac{V_0^2}{2M^2} \int_{E \leq \epsilon_{HOMO}} dE \int_{E' \geq \epsilon'_{LUMO}} dE' \frac{\rho(E) \rho'(E')}{(E_{n'} - E_n)^2} \\ &\times \sum_{i, j \in S_M} \psi_{Ei}^* \psi_{E'i} \psi_{Ej} \psi_{E'j}^*, \end{aligned} \quad (6)$$

which depends explicitly both on the density of states (DOS) with and without impurity, $\rho'(E')$, $\rho(E)$ and on the wave function amplitudes with and without the impurity $\psi_{E'i}, \psi_{Ei}$. We note that, since the number of fermions N is kept fixed, the Fermi energy of the pure system ϵ_F can be different from the one of the system with the perturbation ϵ'_F , since all energy levels $E_{n'}$ may change with the

perturbation. We therefore find it convenient to define the highest occupied energy level without the perturbation as ϵ_{HOMO} and the lowest unoccupied energy level with the perturbation as ϵ'_{LUMO} . We note that Eq. (6) is still an exact representation of the Anderson integral, rewritten in terms of the density of states. As the density of states of the AA model is known to show fractal behavior at the critical point $\lambda_c = 2$, let us first consider the effect of the impurity on the energy spectrum.

IV. ENERGY SPECTRUM

In Fig. 2 (a) we show the energy level spectrum of the AA model, Eq. (3) for $b = 0$ and the critical parameter $\lambda_c = 2.0$ as function of filling factor n . The dashed line indicates the filling of $n = 0.309$, corresponding without an impurity to the Fermi energy $E_F/J = -1.923$. In the inset the zoomed energy interval close to that filling $n = 0.309$ is seen to correspond to a region of large density of states. For a single site impurity the energy level spectrum is plotted for three different impurity strength V_0 as displayed by the colored symbols, respectively. Fig. 2 (b) and (c) show a full and zoomed energy level diagram, with and without impurity. The case without impurity is drawn in a grey color. While the energy bands are not shifted, the formation of bound states outside of the energy bands is seen even for the weakest impurity strength. Fig. 2 (d) shows the density of state (DOS) as a function of energy close to Fermi energy. The results presented here are randomly chosen from one of the realizations. For the calculation of the DOS a broadening $\eta = 1. \times e^{-5}$ has been used.

Fig. 18 shows the average density of states as function of energy E , as averaged over the random phases ϕ in the Hamiltonian Eq. (3) for $b = 0$ and $\lambda = 2$ of 200 realizations. This supports the observation that the energy bands are not shifted by more than a level spacing, and that the formation of bound states outside of the energy bands is seen even for the weakest impurity strength.

V. GROUND STATE FIDELITY OF THE AA-MODEL WITH A SINGLE SITE IMPURITY

A. Numerical Results

Let us first consider the fidelity in the 1D Aubry-André model with Hamiltonian Eq. (3) for $b = 0$, for a single site impurity, $M = 1$, Eq.(4), numerically. Calculating the fidelity, using its definition $F = |\langle \psi' | \psi \rangle|$, we plot in Fig. 3 (a), (b) the average fidelity $F_{\text{ave}} = \langle F \rangle$ and the typical fidelity as function of length L for different impurity strengths $V_0 = 0.1, 0.01$. Here, we defined $F_{\text{typ}} = \exp \langle \log F \rangle$, where $\langle \dots \rangle$ denotes the average over 1000 realizations of a uniform random phase in $[0, 2\pi)$. We find that both the average and the typical fidelity

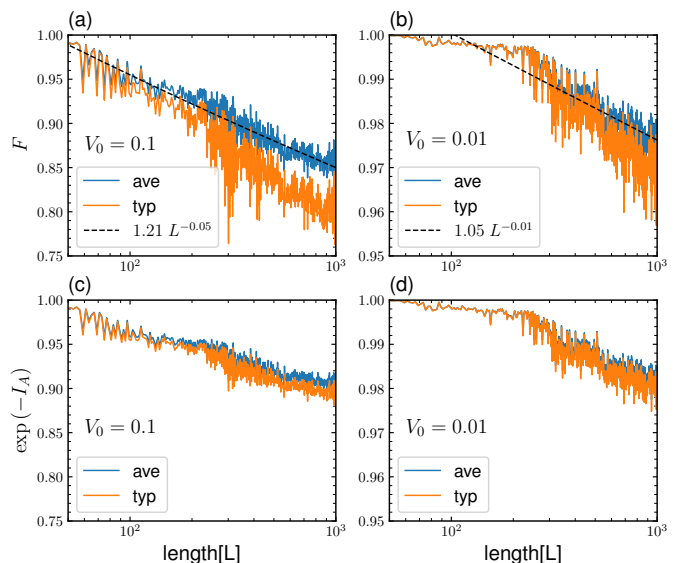


FIG. 3: (a) Average and typical fidelity as function of length L with a single impurity of strength $V_0 = 0.1$ and (b) for $V_0 = 0.01$. The dashed line is a fitted power law as given in the legend. (c) Average and typical value of $\exp(-I_A)$, where I_A is the Anderson integral Eq. (5) for $V_0 = 0.1$ and (d) for $V_0 = 0.01$. Parameter $\lambda_c = 2.0$, data averaged over 1000 sample realizations.

decay with a power law, and not exponentially. The typical fidelity is smaller than the average one for all system sizes L . This difference becomes more pronounced with stronger impurity strength V_0 , while the fidelity becomes smaller with increasing V_0 overall. For comparison, we also calculated the Anderson integral I_A , and plot in Fig. 3 (c), (d) the average of its exponential $\langle \exp(-I_A) \rangle$, which should give according to Eq. (1) the upper bound of the average fidelity, and the exponential of the average I_A , $\exp(-\langle I_A \rangle)$, which corresponds to the upper bound for the typical fidelity. Indeed, we confirm the inequality Eq. (1) for both impurity strengths $V_0 = 0.1, 0.01$. But we observe that the typical fidelity F_{typ} is substantially smaller than its upper bound $\exp(-\langle I_A \rangle)$.

B. Anderson Integral: Analytical Results

These numerical results are in contradiction with the prediction of an exponential orthogonality catastrophe, as found by an analytical derivation in Ref.⁸ at a quantum critical point, where the coupling to a continuum of excited states due to the impurity was found to be enhanced by quantum critical power law correlations. Let us therefore reconsider the derivation of the Anderson integral for critical states.

In fact, in the critical regime all wavefunctions are multifractal¹⁷ and the correlation function of intensities associated to two energy levels distant in energy by

$\omega_{nm} = E_n - E_m$ is enhanced, as given by^{18–20}

$$C(\omega_{nm} = E_n - E_m) = L^d \int d^d r \langle |\psi_n(\mathbf{r})|^2 |\psi_m(\mathbf{r})|^2 \rangle = \begin{cases} \left(\frac{E_c}{\text{Max}(|\omega_{nm}|, \Delta)} \right)^{\eta/d}, & 0 < |\omega_{nm}| < E_c, \\ \left(\frac{E_c}{|\omega_{nm}|} \right)^2, & |\omega_{nm}| > E_c, \end{cases}, \quad (7)$$

where Δ is the average level spacing at the Fermi energy. The power is given by $\eta = 2(\alpha_0 - d)$, with multifractality parameter α_0 and the dimension d . For the critical AA model, the power is known to be $\eta = 1/2$.²¹ Since all its states are critical, the correlation energy E_c is of order of the band width D . For $|\omega_{nm}| < E_c$ correlations are thus indeed enhanced in comparison to the plane-wave limit $C_{nm} = 1$. Note, that for $|\omega_{nm}| > E_c$ it decays below 1.

Mean Value of the Anderson Integral.— If we assume that the perturbed eigenstates $\langle n' |$ in Eq. (5) can be replaced by an eigenstate without the impurity, $\langle n |$, we can insert the correlation function Eq. (7) into Eq. (5) to calculate the mean value of I_A , and find for a single site impurity, $M = 1$,

$$\langle I_A \rangle = \frac{V_0^2}{2} \iint_{\epsilon < \epsilon_{\text{HOMO}}, \epsilon' > \epsilon_{\text{LUMO}}} d\epsilon d\epsilon' \rho(\epsilon) \rho(\epsilon') \frac{C_{\epsilon, \epsilon'}}{(\epsilon - \epsilon')^2}. \quad (8)$$

This gives an estimate for the upper bound of the typical average of F , $\exp(\langle \ln F \rangle) \leq \exp(-\langle I_A \rangle)$. Assuming furthermore that the density of states is only slowly varying $\rho(E) \approx \rho(E_F) = \rho_0$, and denoting the level spacing at the Fermi energy $\Delta = \epsilon_{\text{LUMO}} - \epsilon_{\text{HOMO}}$, we get at the AMIT with Eq. (7)

$$\langle I_A \rangle|_{E_F=E_M} = \frac{(\rho_0 V_0)^2}{2\gamma(1+\gamma)} \left(\frac{E_c}{\Delta} \right)^\gamma, \quad (9)$$

depending on E_c/Δ with power $\gamma = \eta/d$. For the critical phase of the 1-dimensional AA model, $d = 1$, $\gamma = 1/2$.²¹

Since all states are critical at $\lambda = 2$, we set the correlation energy to the band width $E_c = D$. In a metal the average level spacing is $\Delta = 1/(\rho_0 L)$. Note, however that for the spectral spectrum of the AA model, the level spacing at the Fermi energy scales with L rather as $\Delta(L) \sim L^{-z}$, with $z > 1$.¹⁵ Thereby, we get

$$\langle I_A \rangle|_{E_F=0} = \frac{\rho_0^2 V_0^2}{2\gamma(1+\gamma)} (D\rho_0 L^z)^\gamma. \quad (10)$$

Thus, we get with $\gamma = \eta/d = 1/2$, $\rho_0 = 1/D$, that the Anderson integral diverges as a power low with system size L

$$\langle I_A \rangle|_{E_F=0} = \frac{2V_0^2}{3D^2} L^{z/2}, \quad (11)$$

and thus the typical fidelity decays exponentially with the system size, the exponential orthogonality catastrophe, in agreement with Ref..⁸

In the metallic regime $\lambda < 2$ one rather gets

$$\langle I_A^M \rangle|_{E_F=0} = \frac{\rho_0^2 V_0^2}{2} \ln(D\rho_0 L). \quad (12)$$

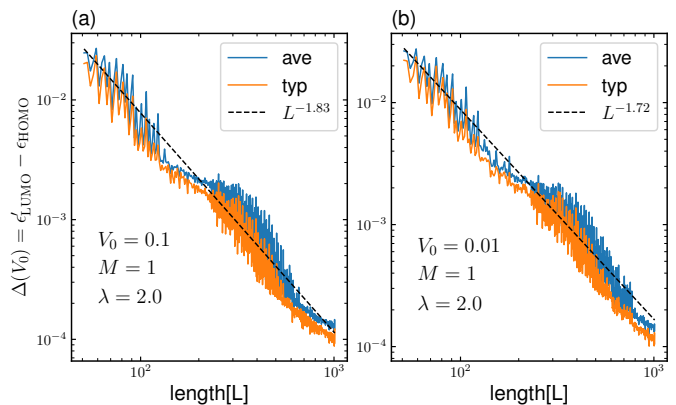


FIG. 4: Average and typical gap, the difference between HOMO and LUMO energies Eq. (13) of the model before and after quench were considered) for two different single impurity strengths (a) $V_0 = 0.1$ and (b) $V_0 = 0.01$. In all results, we fix parameter $\lambda = 2.0$ and data averaged over 1000 sample realizations.

Thus, in order to be able to distinguish the exponential decay of the typical fidelity due to critical correlations, Eq. (11) in comparison to the noncritical result Eq. (12) the system size L should be so large that $4/3L^{z/2} > \ln L$ which is indeed valid for all $L > 1$ for $z > 1$. Thus, according to this result, the numerical calculations should see the exponential decay, if the analytical derivation is valid. Therefore, let us reconsider the approximations yielding to the result Eq. (10), in order to find out the reason for this discrepancy with the numerical results.

C. Anderson Integral: beyond perturbation theory.

1. As the energy levels are modified by the perturbation, the gap between the lowest occupied state with the perturbation and the highest occupied level without perturbation depends itself on the disorder potential V_0 ,

$$\Delta(V_0) = \epsilon'_{\text{LUMO}} - \epsilon_{\text{HOMO}}. \quad (13)$$

Since it provides the infrared cutoff to the integrals in the Anderson integral, we thereby find in the critical phase

$$\langle I_A \rangle|_{E_F=E_M} = \frac{(\rho_0 V_0)^2}{2\gamma(1+\gamma)} \left(\frac{E_c}{\Delta(V_0)} \right)^\gamma, \quad (14)$$

In Fig. 4 the average and typical gap $\Delta(V_0)$, Eq. (13) is shown for two different single impurity strengths, namely (a) $V_0 = 0.1$ and (b) $V_0 = 0.01$ for critical parameter $\lambda = 2.0$ and data averaged over 1000 sample realizations. We see that the magnitude of the gap is not changed by the impurity, so that this weak dependence of $\Delta(V_0)$ on V_0 , does not change the result for the Anderson integral Eq. (11).

Also, as was observed for the gap of the unperturbed system in Ref.,¹⁵ the decay with system size L of the gap $\Delta(V_0)$ is strongly fluctuating with L and does not follow a clear scaling law, even when averaging over 1000 realizations. However, it clearly decays with a power $z > 1$, faster than the average level spacing of a metal.

2. The density of states is affected by the presence of the impurity, as seen in Fig. 2 for a particular realisation of the phase ϕ . As discussed in section IV, the energy bands are hardly shifted, but the formation of bound states outside of the energy bands is found even for the weakest impurity strength. Close to the Fermi energy Fig. 2 (d) shows that the density of state (DOS) is only weakly shifted by the impurity, by the order of the level spacing Δ . As we choose an energy region of large density of states, which is not shifted on average by the impurity, as seen in Fig. 18, we conclude that the small change of DOS $\rho'(E)$ by the impurity does not result into a change of the divergence with system size L of the average Anderson integral in the critical regime, and thus cannot be responsible for the discrepancy with the numerical results.

3. We disregarded in the derivation in section VB the change of wave function intensity at the location of the impurity by the addition of the impurity. For a single site potential impurity at site \mathbf{x} with amplitude V_0 , the perturbed intensity $|\psi_{n'}(\mathbf{x})|^2$ can be written exactly as²²

$$|\psi_{n'}(\mathbf{x})|^2 = \lim_{E \rightarrow E_{n'}} (E - E_{n'}) \frac{V_0(G_E^0(\mathbf{x}, \mathbf{x}))^2}{1 - V_0 G_E^0(\mathbf{x}, \mathbf{x})}, \quad (15)$$

where,

$$G_E^0(\mathbf{x}, \mathbf{x}) = \sum_l |\psi_l(\mathbf{x})|^2 \frac{1}{E - E_l + i\delta}. \quad (16)$$

Performing the limit in Eq. (15) with de l'Hospital, one finds

$$|\psi_{n'}(\mathbf{x})|^2 = |\psi_n(\mathbf{x})|^2 \frac{(1 + \frac{E_{n'} - E_n}{|\psi_n(\mathbf{x})|^2} \sum_{l \neq n} \frac{|\psi_l(\mathbf{x})|^2}{E_{n'} - E_l})^2}{1 + \frac{(E_{n'} - E_n)^2}{|\psi_n(\mathbf{x})|^2} \sum_{m \neq n} \frac{|\psi_m(\mathbf{x})|^2}{(E_{n'} - E_m)^2}} \quad (17)$$

where E_n is the energy level closest in energy to the perturbed energy $E_{n'}$. It depends on the disorder potential only implicitly through the Eigen energy of the perturbed state $E_{n'}$. Since $E_{n'} - E_n$ has a polynomial dependence on the disorder potential V_0 , we can approximate it by the leading term, linear in V_0 , $E_{n'} - E_n \approx V_0 |\psi_n(\mathbf{x})|^2$, yielding

$$|\psi_{n'}(\mathbf{x})|^2 \approx |\psi_n(\mathbf{x})|^2 \frac{(1 + V_0 \sum_{l \neq n} \frac{|\psi_l(\mathbf{x})|^2}{E_{n'} - E_l})^2}{1 + V_0^2 |\psi_n(\mathbf{x})|^2 \sum_{m \neq n} \frac{|\psi_m(\mathbf{x})|^2}{(E_{n'} - E_m)^2}} \quad (18)$$

Inserting this approximation into the Anderson integral, we can check whether these corrections in V_0 change the divergence of the Anderson integral. In the metal phase,

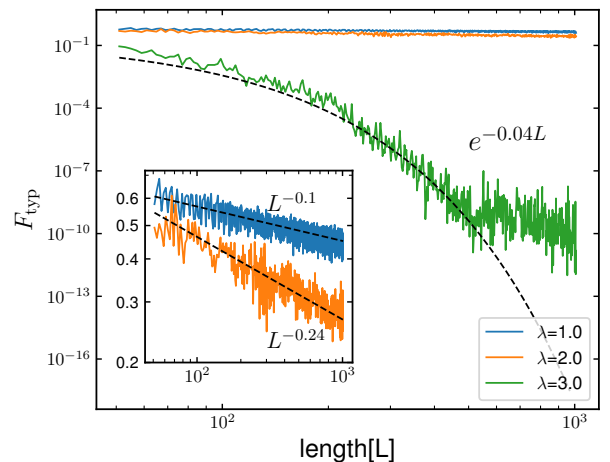


FIG. 5: Typical fidelity $F_{typ} \approx \exp(\langle \log F \rangle)$ of a single impurity with strength $V_0/J = 20$ for different λ parameter in log – log scale. Filling fixed at $n = 0.309$. Inset magnifies results of main panel for $\lambda = 1.0, 2.0$. Results are averaged over 1000 samples. Black-dashed lines are fitted curves.

$|\psi_n(\mathbf{x})|^2 \sim 1/L$ and due to the asymmetry of the summations in the numerator of Eq. (18), we find only weak corrections, which do not change the $\ln L$ –dependence of the Anderson integral in the metallic regime. In the critical regime, however, all wave functions are multifractal, so that the local intensity $|\psi_l(\mathbf{x})|^2$ is widely distributed and may vary strongly with energy E_l . Then, the corrections due to the summations in Eq. (18) both in the numerator and denominator may yield finite results, especially when the intensity of the state at the Fermi energy at the location of the impurity $|\psi_n(\mathbf{x})|^2$ happens to be smaller than in other states. Inserting Eq.(18) into the Anderson integral, we see that multi point correlations of the intensity arise even for the average Anderson integral.

Thus, the average Anderson integral can in general not be reduced to an integral over the pair correlation function Eq. (7). The presence of multipoint correlation may therefore weaken the infrared divergence compared to Eq. (11). The numerical results shown in Fig. 3 in fact provide strong evidence, that the Anderson integral depends on system size only logarithmically, resulting in a fidelity at the critical point which decays with a power law with system size, albeit decaying faster than in the metallic regime. Numerical Results for the fidelity in the presence of an impurity in other quantum critical systems, in particular in random banded matrices²³ and at the 3D Anderson metal-insulator transition²⁴ did not find evidence for an exponential AOC neither, but rather found evidence for a potential AOC. As outlined above, the explanation may be that the corrections to the local intensity at a single site impurity Eq. (18) result in multipoint correlations, which weaken the infrared singularity of the Anderson integral in these quantum critical systems, thereby explaining the numerically observed power law Anderson orthogonality catastrophe.

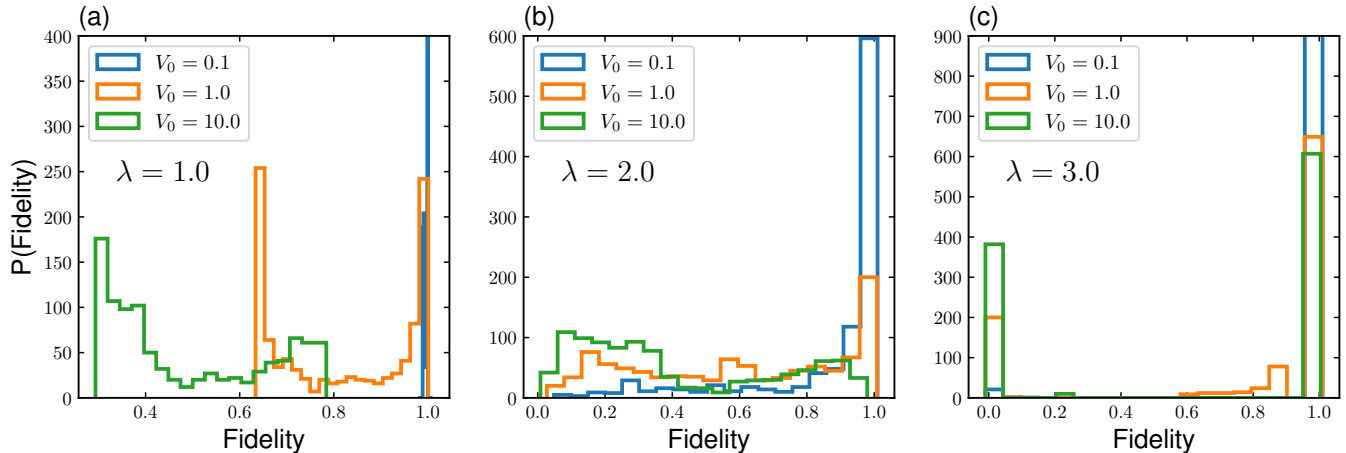


FIG. 6: Distribution of the fidelity for a single impurity $M = 1$ with different strengths. Panels are showing results for three (a) metallic, (b) critical, and (c) localized phases. System size is $L = 1009$ and data are collected from 2000 realizations.

D. Fidelity in the Insulator phase: Statistical Exponential Orthogonality Catastrophe

In Fig. 5 the typical fidelity $F_{typ} = \exp\langle \log F \rangle$ of a strong single impurity with strength $V_0/J = 20$ is shown for the metallic $\lambda = 1.0$, the critical $\lambda_c = 2.0$, and the insulator $\lambda = 3.0$ regime. The filling is kept fixed at $n = 0.309$. All results are obtained by averaging over 1000 samples. We see that both in the metallic and the critical regime, the typical fidelity decays with system size like a power law, albeit the decay is faster in the critical regime. This is seen better in the inset where the dashed lines are fitted curves as indicated.

In the insulator regime $\lambda = 3.0$, however, the fidelity is by orders of magnitude smaller than that in the metallic and critical regimes. Moreover, it decays with system size L exponentially, as seen by the fitted dashed line, until it decays more slowly at system sizes exceeding $L = 500$. In Refs.10,11, an exponential orthogonality catastrophe was found numerically in Anderson-localized Fermi systems, when the perturbation is turned on adiabatically slowly. In Ref.10 that has been explained in terms of a *statistical* orthogonality catastrophe.

Indeed, in the strongly localised regime, when each Eigenfunction is localised on one site only, one obtains a Bernoulli distribution of the fidelity of fixed particle number N , which is either 0 or 1 with probability u , $1 - u$, respectively. The reason is, that in this strongly localised regime a local impurity cannot mix Eigenstates, but only shift the energy of that state, which is located at the site of the impurity. Thereby, for fixed number of particles the impurity may shift an occupied level to higher energies, leaving it unoccupied, while a state at another site becomes occupied, which is orthogonal to the state at the site of the impurity, or vice versa. Thus, by definition of the fidelity at fixed N , the fidelity is then exactly zero. If, on the other hand, the impurity shifts

the energy such that the level remains occupied when it was occupied before, or leaving it unoccupied, when it was unoccupied without the impurity, the fidelity remains exactly one. Thus, one has a statistical distribution which has only two possibly values, $S = 0$ with probability u or $S = 1$ with probability $1 - u$, where $u(V_0)$ is the probability that the impurity shifts the energy level at the site of the impurity from occupied to unoccupied states or vice versa. Thus, while the average fidelity is finite $\langle F \rangle = 1 - u$, the typical fidelity is vanishing, $\exp\langle \ln F \rangle = \exp(-\infty u + 0(1 - u)) = 0$. This statistical mechanism for the reduction of the typical fidelity is thereby completely different from the mechanism for the Anderson orthogonality catastrophe, where it is the coupling to a continuum of states in a metal which leads to the power law suppression of the fidelity.

In Fig. 6 the distribution of the fidelity is shown in the metallic, the critical and the insulator phase for three different impurity strengths. Indeed, in the insulator phase the distribution is bimodal, and the peak around zero fidelity is increasing with impurity strength V_0 , approaching a Bernoulli distribution, with only small weight at intermediate values of the fidelity. In contrast, in the critical phase the distribution of F is very wide spreading over all values of F , where the weight of small fidelity increases with V_0 . The distribution of F in the metal phase on the other hand has a finite width, is bimodal, and becomes shifted to smaller F as V_0 is increased.

Having understood the distribution of F , let us next try to explain the exponential suppression of the fidelity with system size L in the insulator phase. As the filling factor $n = N/L$ is fixed as the system size L is increased, the number of occupied levels N increases. However, in the strongly localised regime, the probability that the single state at the site of the impurity is shifted from occupied to unoccupied levels of vice versa, the probability u , does not change with L , since it is only a function of

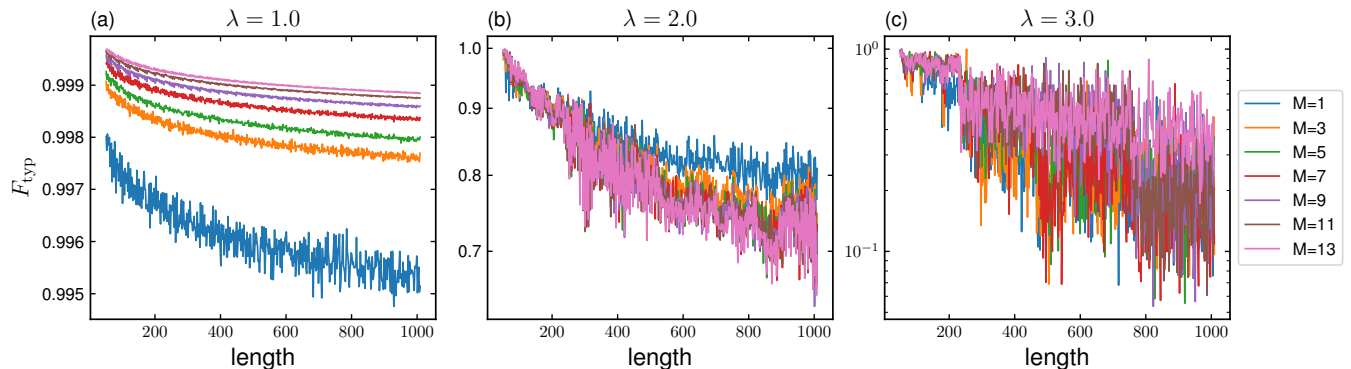


FIG. 7: Typical fidelity at filling $n = 0.309$ as function of length L (a) for the metallic phase $\lambda = 1$, (b) for the critical phase $\lambda = 2$, and (c) for the insulator phase $\lambda = 3$. Results for different extensions of the impurity M are shown in color at fixed strength of the impurity $V_0 = 0.1J$, sampled over 1000 realizations.

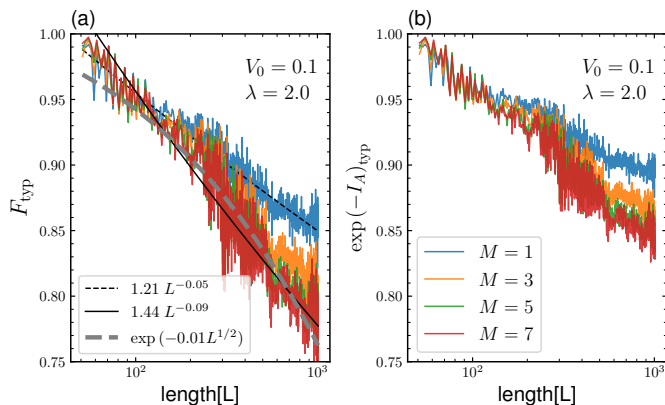


FIG. 8: (a) and (b) show typical Fidelity and Anderson integral, respectively, as function of length L for different numbers of impurity sites M for a fixed impurity strength $V_0 = 0.1$ for the AA model at the critical point $\lambda = 2.0$ and averaged over 1000 sample realizations.

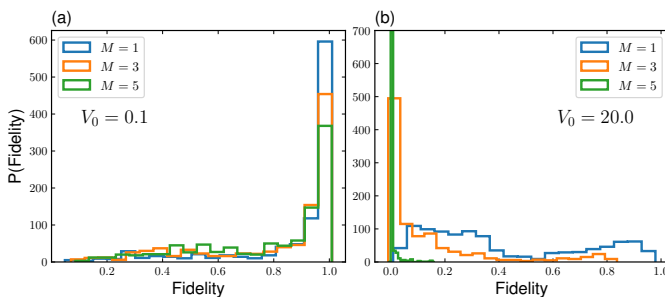


FIG. 9: The distribution of the fidelity F in the critical phase $\lambda = 2.0$ for impurity strength (a) $V_0 = 0.1$ and (b) $V_0 = 20$, averaged over 1000 realizations, for systems size $L = 1024$.

the impurity strength V_0 , whether the energy level shift is sufficiently strong and the typical fidelity remains zero for all sizes. Thus, in the limit of strong single site localisation, the typical fidelity would be zero for all system

sizes $L \gg 1$.

When the localisation is not as strong, however, each localised state is extended over several sites, within the range of a localisation length ξ . Thus, an impurity located within this range may mix the localised state with a finite number of other states. According to the Anderson mechanism, that would yield a finite fidelity on average, since an impurity can only be coupled to a finite number of states, which does not change as the system size increases. This is the reason that in Ref.8 a finite typical fidelity, independent of the system size has been found analytically. However, due to the statistical mechanism, which was not considered in Ref.8, the impurity may shift an occupied state up in energy so that it becomes unoccupied, or vice versa. Then, another single particle state becomes occupied which may be (almost) orthogonal to the previously occupied state without the impurity. As the system size increases beyond a typical localisation length ξ , the fidelity is decaying exponentially due to this statistical mechanism. As there is typically an exponentially small but finite hybridisation matrix elements between all sites, in reality the impurity may couple to a larger amount of states even though with exponentially small amplitude. This might explain that the typical fidelity seems to saturate to a very small but finite value at large system size L in Fig. 5.

VI. FIDELITY WITH EXTENDED IMPURITY - CRITICAL EXPONENTIAL AOC

Next, we explore how the fidelity depends on the extension of the impurity at fixed total strength V_0 , as defined by the impurity Hamiltonian Eq. (4). Clearly, in the limit when it extends over the whole system $M = L$, the Eigenstates are not changed, and only the total energy is shifted by V_0/L , so that the fidelity is equal to one. Thus, one may expect that the fidelity increases as the the extension of the impurity M is increased at

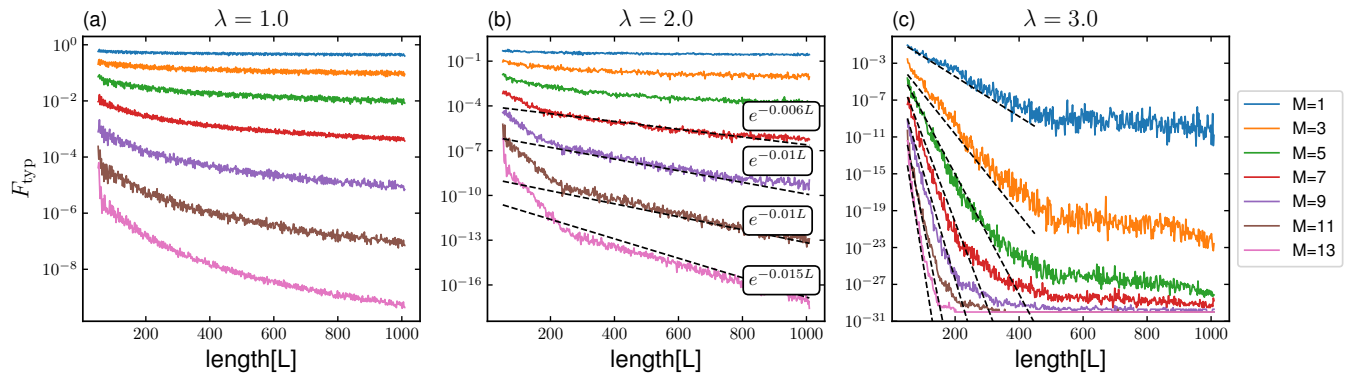


FIG. 10: Typical fidelity at filling $n = 0.309$ as function of lattice length. Panels (a), (b), and (c) show results for different values of λ as the model is in the extended, critical, and localized phases, respectively. In each panel, different data are shown in the color corresponding to the number of impurity sites M , while the amplitude of impurity is fixed at $V_0 = 20J$, sampled over 1000 realizations. The dashed lines are the linear fit corresponding to exponential decay.

fixed total strength V_0 . In fact, this is what happens for a periodic 1D tight binding model for a weak impurity potential $V_0 = 0.1$, as seen in Fig. 16 in Appendix C, where the typical value of the fidelity and the upper bound $\exp(-I_A)$ are plotted as function of chain length L for different impurity extensions M . The typical fidelity increases with M , decaying more slowly with a power law of L , the larger M is. Similarly, in the metallic phase of the AA model for a weak impurity potential $V_0 = 0.1J$, the typical and average fidelity become larger and decay more slowly with L as M is increased, as seen in Fig. 7 (a), and in appendix D Fig. 19 (a), respectively, in accordance with the expectation formulated above. Averaging Eq. (5) over the phase ϕ we get the average Anderson integral for the extended impurity as

$$I_A = \frac{V_0^2}{2M^2} \sum_{n=1}^N \sum_{n'>N} \sum_{i,j \in S_M} \langle \frac{\psi_{ni}^* \psi_{n'i} \psi_{n'j}^* \psi_{nj}}{(E_{n'} - E_n)^2} \rangle_{\phi}, \quad (19)$$

As the phase difference of the wave function amplitude between different sites varies with ϕ , averaging over the phase ϕ gives $\langle \psi_{ni} \psi_{n'j}^* \rangle_{\phi} \approx \delta_{ij} |\psi_{ni}|^2$, so that we find in the metallic regime, where $|\psi_{ni}|^2 \sim L^{-1}$ that $I_A = 1/(2M)\rho_0^2 V_0^2 \ln N$, decaying with M , resulting in an increased fidelity with larger M , in qualitative agreement with the numerical results for the typical fidelity in the metallic regime, Fig. 7 (a).

In stark contrast to this, we find that in the critical phase of the AA-model the fidelity is diminished more strongly with increasing extension M of the impurity, as seen in Fig. 7 (b) where the typical fidelity is plotted, as well as in the Appendix C Fig. 19 (b), where average fidelity is plotted, as function of length L for different extensions M for a fixed, weak impurity strength $V_0 = 0.1$ at the critical point $\lambda = 2.0$, averaged over 1000 sample realizations. Results at the critical point $\lambda = 2.0$, are replotted in a semi-logarithmic plot in Fig. 8 (a) for the typical Fidelity and in Fig. 8 (b) for the Anderson integral as function of length L for different

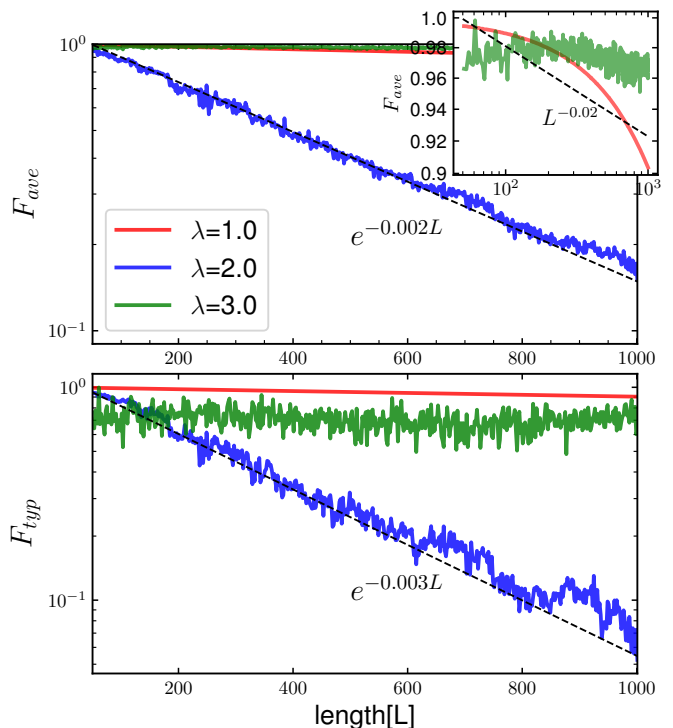


FIG. 11: Average (top) and typical (bottom) fidelity after a parametric perturbation in Eq.(3) with change $\delta\lambda = 0.1$, for the metallic phase $\lambda = 1$, critical phase $\lambda = 2$, and insulator phase $\lambda = 3$ in solid-colored lines. The dashed-black line are the fitted curves as indicated. Filling factor fixed at $n = 0.309$, and averaged over how 1000 samples.

impurity extension M for a fixed weak impurity strength $V_0 = 0.1$, averaged over 1000 sample realizations. Fits to power law and exponential dependence on L are plotted as indicated. For the largest extension $M = 7$ an exponential decay cannot be excluded. Thus, we may recover the analytically predicted exponential AOC in

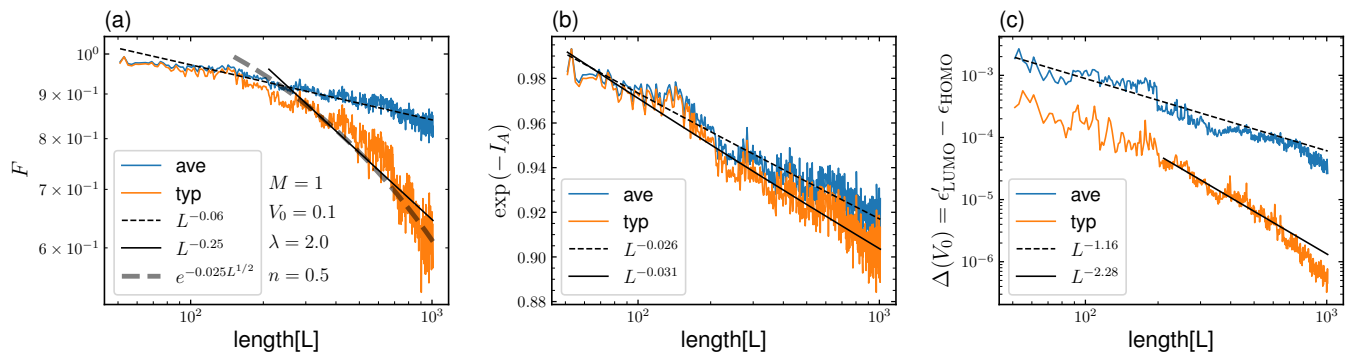


FIG. 12: For a single site impurity $M = 1$ in the extended AA-model at the mobility edge for $\lambda_c = 2.0$, corresponding to half filling $n = 0.5$ (a) average and typical fidelity as function of length L with a single impurity of strength $V_0 = 0.1$. The dashed and solid lines are fits to power laws, as given in the legend. (b) average and typical value of $\exp(-I_A)$, where I_A is the Anderson integral Eq. (5). (c) average and typical value of the gap $\Delta(V_0)$, Eq. (13) as function of system size L . The dashed and solid lines are fits to power laws, as given in the legend. All results are averaged over 1000 sample realizations.

the critical phase,⁸ albeit only for an extended impurity. A possible explanation is that the magnitude of multi-point correlations, which we found to be responsible for masking the critical two point correlations, may become diminished, for the extended impurity, so that the critical enhancement of two point correlations dominate the typical fidelity for extended impurity, resulting in the exponential AOC in the critical phase. To get a better understanding of the result in the critical phase let us look at the distribution of the fidelity F in the critical phase $\lambda = 2.0$. For impurity strength $V_0 = 0.1$ averaged over 1000 realizations, for systems size $L = 1024$ the distribution is shown in Fig. 9 (a). The distribution of the fidelity is found to be wide, as expected in the critical phase.⁸ The probability that the ground state is not affected by the impurity, that the fidelity is close to one, is found to decrease with increasing M .

In the insulator phase $\lambda = 3$ for a fixed weak impurity strength $V_0 = 0.1$ the fidelity is decaying more strongly than in the other phases. With increasing extension M of the impurity the fidelity becomes larger, as seen in Fig. 7 (c) and Fig. 19 (c), where the typical fidelity and average fidelity are plotted, respectively, as function of length L for different M averaged over 1000 sample realizations. The reason for that behavior might be that the effect on single site localised states is smaller for an extended impurity, thereby diminishing the probability u that an occupied state becomes shifted to unoccupied states as the impurity is turned on, enhancing thereby the fidelity, according to the theory of the statistical exponential AOC as outlined in section VD.

For an extended impurity with strong amplitude $V_0 = 20J$, we find that the AOC is clearly exponential in the critical phase as seen in Fig. 10 (b) for extension $M \gg 1$. We find that the larger the extension M , the more the fidelity becomes diminished and the stronger the exponential AOC becomes. This is confirmed by the distribution of the fidelity for such a strong impurity in the critical

phase, as shown in Fig. 9 (b).

In the metallic phase a strong impurity $V_0 = 20J$ is found to reduce the fidelity more strongly with increasing M , but the typical fidelity Fig. 10 (a) and average fidelity Fig. ?? (a) continue to decay with a power law in L for all M . A similar behavior is found for a strong impurity in the tight binding model as shown in Appendix C, Fig. 17.

In the insulator phase Fig. 10 (c) and Fig. 20 (c) shows a strong exponential AOC for the typical and average fidelity respectively, which becomes stronger with the extension M of the impurity.

VII. FIDELITY WITH PARAMETRIC PERTURBATION - PARAMETRIC EXPONENTIAL AOC

The concept of fidelity has been generalized to parametric perturbations of a quantum system. It have been successfully used to characterize quantum phase transitions.⁵ Therefore, let us next study a perturbation which shifts the parameter λ by a small amount $\delta\lambda$

$$H_{Pert} = \delta\lambda \sum_{i=1}^L \cos(2\pi Qi + \phi) c_i^+ c_i. \quad (20)$$

The effect of such a parametric quench has been recently studied in the AA-model in Ref³⁰ by calculating the so called fidelity susceptibility $\chi_F(\lambda) = \lim_{\delta\lambda \rightarrow 0} -2 \log F / \delta\lambda^2$. We note that, an upper bound for the fidelity susceptibility $\chi_F(\lambda)$ is given by the Anderson Integral,

$$\begin{aligned} \chi_F(\lambda) &\leq \lim_{\delta\lambda \rightarrow 0} 2I_A / \delta\lambda^2 \\ &= \lim_{\delta\lambda \rightarrow 0} \frac{1}{\delta\lambda^2} \sum_{n=1}^N \sum_{n' > N} \frac{|\langle n | H_{Pert} | n' \rangle|^2}{(E_{n'} - E_n)^2} \end{aligned} \quad (21)$$

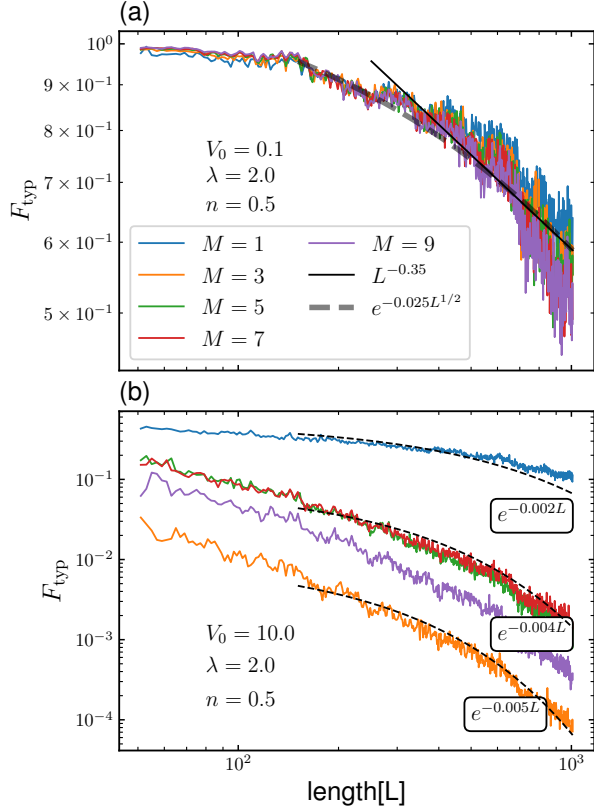


FIG. 13: Typical fidelity for an extended impurity for the extended AA-model at the mobility edge for $\lambda_c = 2.0$, corresponding to half filling $n = 0.5$, versus length L for different extension M . Impurity strength (a) $V_0 = 0.1$, and (b) $V_0 = 10$. All data averaged over 1000 sample realizations. Fitted curves are shown in solid or dashed black lines

$$= \sum_{n=1}^N \sum_{l>N} \sum_{i,j} \frac{\cos(2\pi Qi + \phi) \cos(2\pi Qj + \phi) \psi_{ni}^* \psi_{nj} \psi_{li} \psi_{lj}^*}{(E_l - E_n)^2},$$

where the indices n, l denote the unperturbed Eigenstates.

In the critical phase, noting that local intensities are power law correlated in energy, the dominating contributions come from the terms at the same locations $i = j$. Thus we find

$$\chi_F(\lambda) \leq \sum_{n=1}^N \sum_{l>N} \sum_i \frac{\cos(2\pi Qi + \phi)^2 |\psi_{ni}|^2 |\psi_{li}|^2}{(E_l - E_n)^2}. \quad (22)$$

Averaging over the phase ϕ we thereby find approximating $\rho(E) \approx \rho_0$, and using $\Delta = \Delta_0 L^{-z}$

$$\chi_F(\lambda) \leq \frac{1}{2} \frac{\rho_0^2}{\gamma(1+\gamma)} \left(\frac{D}{\Delta_0} L^z \right)^\gamma \sim L^{z\gamma} \quad (23)$$

where for the AA model in the critical phase $\lambda_c = 2$, $\gamma = 1/2$.

Fig. 11 shows the results for average (upper figure) and typical (lower figure) fidelity of a parametric perturbation with $\delta\lambda = 0.1$. As shown, in the metallic phase $\lambda < 2$ we find a power-law decay in the average and typical fidelity, both with the same power, scaling with L as $L^{-0.02}$.

At the critical point $\lambda_c = 2$ the average and typical fidelity are clearly found to decay exponentially. The average fidelity is found to decay as $F_{ave} \sim e^{-0.002L}$ and the typical as $F_{typ} \sim e^{-0.003L}$. Thus, this gives for the typical fidelity susceptibility $\chi_F \approx 0.6L$, in good agreement with the analytical upper bound Eq. (23), which gives with $\gamma = 1/2$, $\chi_F < 2/3 L^{z/2}$, where z is the dynamical exponent, which we found numerically to be close to $z \approx 2$.

Using another approach near the quantum critical point $\lambda_c = 2$, it was recently argued that the fidelity susceptibility scales with system size as $\chi_F(\lambda_c) \sim N^{2/\nu}$,³⁰ where ν is the correlation length critical exponent, given by $\nu \approx 0.89$ according to Ref.31 and by $\nu \approx 0.95$ according to Ref.32, which is also in some agreement with our numerical results.

In the localized phase $\lambda = 3$ both the average and typical fidelity show a very weak and strongly fluctuating dependence on L .

VIII. FIDELITY IN THE EXTENDED AA MODEL

The extended AA (EAA)-model with Hamiltonian Eq. (3) for $b > 0$ has a mobility edge, as seen in Fig. 1 (right) where the inverse participation ratio is plotted as function of energy and parameter λ for the EAA-model where a mobility edge (black solid line) separates the extended phase with $\text{IPR} \rightarrow 0$ from the localized $\text{IPR} \rightarrow a/\xi$, where ξ is the localization length and a the lattice spacing. Let us therefore explore whether there is a critical exponential AOC at the mobility edge, as found analytically in Ref.⁸ at a mobility edge.

First we address the case with a single site impurity $M = 1$ with weak potential $V_0 = 0.1$. In our calculation we set $b = 0.2$ and $\lambda = 2.0J$. We choose half filling $n = N/L = 0.5$ so that the Fermi energy is at the mobility edge $E_{mb} = 0$, see Fig. 1. In Fig.12 we plot both the average and typical fidelity. The fit with a power law in system size L is good for the average fidelity. The typical fidelity shows a much smaller value for all system sizes with a stongrt decay with L . The decay becomes stronger at larger L possibly indicating an exponential AOC.

Compared with the single site impurity with weak potential $V_0 = 0.1J$ in the AA model, $b = 0$, in the critical phase $\lambda_c = 2$, shown in Fig. 3) (a), the average fidelity is of similar magnitude as in the EAA model at the mobility edge Fig.12, while the typical fidelity is smaller and decays faster in the EAA model at the mobility edge Fig.12.

We depicted the average and typical value of $\exp(-I_A)$ in Fig.12 (b) and find that it gives as expected an upper bound for the fidelity for the whole range of systems sizes explored. But we note that the difference between the average and typical value is not as profound as for the fidelity.

We also plot the average and typical gap, the difference between HOMO and LUMO energies $\Delta(V_0)$, Eq.(13) for the extended AA model at the mobility edge in Fig. 12 (c). For both average and typical, we find a power law decay with L with dynamical exponent $z > 1$. Interestingly, the decay of the gap is stronger for the typical than the average gap, which is in contrast to the result for the gap Eq. (13) in the critical regime in the AA model, where the average and typical gap showed a similar magnitude and decay, see Fig. 4.

Finally, let us consider the fidelity in the EAA model at its mobility edge with an impurity extended over M sites. In Figs. 13 (a) and (b) we present the typical fidelity for two impurity strengths $V_0 = 0.1$ and $V_0 = 10$, respectively. For the weak impurity $V_0 = 0.1$ the typical fidelity decays with a power law decaying with system sizes to smaller values the larger the extension of the impurity M is. Thus, this is a similar behavior as we have observed for a weak impurity in the critical AA-model in Fig.7. For the strong impurity we observe in Fig. 13 (b) a smaller typical fidelity decaying exponentially with system size, similarly as for a strong impurity in the critical AA-model in Fig.10 (b).

IX. CONCLUSION

We presented evidence for the exponential orthogonality catastrophe in the (extended) Aubry-André (AA)-Model with an added potential impurity, as function of the size of that impurity. While we not find a predicted exponential AOC in the critical regime for a weak single site impurity, but rather find that the fidelity decays with a power law, in the critical phase. Even though it is found to be smaller and decays faster than in the metallic phase, it does not decay exponentially as predicted. For an extended impurity, however, we find indications of an exponential AOC at the quantum critical point of the AA model and at the mobility edge of the extended AA model and suggest an explanation for this finding. By reexamination of the analytical derivation we identify nonperturbative corrections due to the impurity potential and multipoint correlations among wave functions as possible causes for the absence of the exponential AOC in the critical phase.

We find a different kind of exponential AOC in the insulator phase for which we give a statistical explanation, similar to that it was given in¹⁰ for an adiabatic perturbation in an insulator phase, a mechanism which is profoundly different from the AOC in metals, where it is the coupling to a continuum of states which yields to

the power law suppression of the fidelity.

Furthermore we consider a parametric perturbation to the AA model, and find an exponential AOC numerically, in agreement with an analytical derivation which we provide here.

It has been suggested that the orthogonality catastrophe can be studied in ensembles of ultracold atoms in a controlled way.⁷ Indeed, since the extended AA model was introduced and suggested to be experimentally realised in atomic optical lattices and photonic wave guides,¹⁴ it was recently realized in synthetic lattices of laser-coupled atomic momentum modes, and demonstrated to have a mobility edge.¹⁶ We therefore hope that our analysis will provide guidance for the experimental study of the fidelity and the AOC in these systems. Furthermore, this opens new pathways for the study of nonequilibrium quantum dynamics. We note that our results can be extended to interacting disordered fermion systems, as multifractality exists even in strongly interacting disordered systems.³³

Acknowledgement. We gratefully acknowledge the support from Deutsche Forschungsgemeinschaft (DFG) KE-807/22-1. We thank Eugene Demler for stimulating discussions, initiating this study and Keith Slevin for stimulating discussions and useful comments.

A. Appendix

When the single particle states of a Fermi system are $|n\rangle = c_n^+|0\rangle$, the ground state of N fermions is given by $|\psi\rangle = \prod_{n=1}^N c_n^+|0\rangle$. Adding an impurity the single particle states are changed to $|n'\rangle = c_{n'}^+|0\rangle$, so that the ground state becomes $|\psi'\rangle = \prod_{n'=1}^N c_{n'}^+|0\rangle$. The fidelity is given by the absolute value of the scalar product, $F = |\langle\psi|\psi'\rangle| = |\langle 0|\prod_{n=1}^N c_n \prod_{n'=1}^N c_{n'}^+|0\rangle|$. Defining the scalar product of single particle states of the pure system and the system with perturbation, $A_{nn'} = \langle n|n'\rangle$, and applying the anticommutation relations for c_n, c_n^+ , we can write the fidelity as

$$F = |\det_{n,n' \leq N} A|. \quad (24)$$

$A_{nn'}$ is for fixed n a normalized vector with $\sum_{n'} |A_{nn'}|^2 = 1$, However, since the summation in the fidelity F is restricted, and $|n'\rangle = \sum_{n \leq N} A_{nn'}|n\rangle + \sum_{n > N} A_{nn'}|n\rangle$, only those vector components with $n \leq N$ contribute to the fidelity F . This means that the determinant is taken of a square matrix with column vectors which are not normalized. However, we can normalize each column vector, by multiplying it with $c_{n'} = (1 - \sum_{n > N} |A_{nn'}|)^{-1/2}$ and get the identity

$$F = \prod_{n' \leq N} (1 - \sum_{n > N} |A_{nn'}|^2)^{1/2} \det(A \prod_{n' \leq N} c_{n'}). \quad (25)$$

Since the second factor is now a determinant with normalized column vectors, it cannot exceed one, but can be

smaller, so that $\det(A \prod_{n' \leq N} c_{n'}) < 1$, and therefore

$$\begin{aligned} F &< \prod_{n' \leq N} (1 - \sum_{n > N} |A_{nn'}|^2)^{1/2} \\ &< \exp(-\frac{1}{2} \sum_{n' \leq N} \sum_{n > N} |A_{nn'}|^2). \end{aligned} \quad (26)$$

B. Appendix

When the unperturbed system has the Hamilton operator H_0 with Eigenstates $|n\rangle$ determined by the Schrödinger equation $H_0|n\rangle = E_n|n\rangle$, adding an impurity with Hamiltonian H_{imp} , Eq. (4) with potential strength V_0 changes the Eigenstates to $|n'\rangle$ as determined by $(H_0 + H_{\text{imp}})|n'\rangle = E_{n'}|n'\rangle$. Multiplying by left with $\langle n|$ we thus get the identity

$$\langle n|n'\rangle = \frac{1}{E_{n'} - E_n} \langle n|H_{\text{imp}}|n'\rangle. \quad (27)$$

Thus for a local impurity $V = V_0\delta(\mathbf{r} - \mathbf{x})$, we find

$$\begin{aligned} I_A &= \frac{1}{2} \sum_{n \leq N, n' > N} |\langle n|n'\rangle|^2 \\ &= \frac{1}{2} \sum_{n \leq N, n' > N} \frac{1}{(E_{n'} - E_n)^2} |\langle n|V|n'\rangle|^2 \\ &= \frac{V_0^2}{2} \sum_{n \leq N, n' > N} \frac{|\psi_n(\mathbf{x})|^2 |\psi_{n'}(\mathbf{x})|^2}{(E_{n'} - E_n)^2}, \end{aligned} \quad (28)$$

where $|\psi_n(\mathbf{x})|^2 = |\langle n|\mathbf{x}\rangle|^2$, $|\psi_{n'}(\mathbf{x})|^2 = |\langle n'|\mathbf{x}\rangle|^2$, is the intensity with and without the additional impurity at position \mathbf{x} .

For a single site potential impurity at site \mathbf{x} with amplitude V_0 , the perturbed intensity $|\psi_{n'}(\mathbf{x})|^2$ can be written as²²

$$|\psi_{n'}(\mathbf{x})|^2 = \lim_{E \rightarrow E_{n'}} (E - E_{n'}) \frac{V_0(G_E^0(\mathbf{x}, \mathbf{x}))^2}{1 - V_0 G_E^0(\mathbf{x}, \mathbf{x})}, \quad (29)$$

where,

$$G_E^0(\mathbf{x}, \mathbf{x}) = \sum_l |\psi_l(\mathbf{x})|^2 \frac{1}{E - E_l + i\delta}. \quad (30)$$

Performing the limit using de l'Hospital, one finds

$$|\psi_{n'}(\mathbf{x})|^2 = \frac{(\sum_l \frac{|\psi_l(\mathbf{x})|^2}{E_{n'} - E_l})^2}{\sum_m \frac{|\psi_m(\mathbf{x})|^2}{(E_{n'} - E_m)^2}}, \quad (31)$$

which depends on the disorder potential only implicitly through the Eigen energy of the perturbed state $E_{n'}$.

Keeping in all summations only the largest terms, which are the terms with the unperturbed Eigen energy E_l closest to $E_{n'}$, we get approximately

$$|\psi_{n'}(\mathbf{x})|^2 = |\psi_l(\mathbf{x})|^2 |_{\min_l (|E_l - E_{n'}|)}, \quad (32)$$

and we recover the result obtained in second order perturbation theory.

C. Appendix

In this appendix, the tight-binding model is revisited numerically as a benchmark. We consider Hamiltonian $H = \sum_i (c_i^\dagger c_i + h.c)$ and introduce the impurity as is defined in the main text Eq.(4).

Fig. 14-(a) shows the energy level spectrum as function of filling factor n for a single impurity $M = 1$ with three different strength V_0 (as displayed by the colored symbols). The dashed line indicates the filling of $n = 0.5$, corresponding without an impurity to the Fermi energy $E_F/J = 0$. Inset shows a zoom close to the Fermi energy. Fig. 14 (b) and (c) show a full and zoomed energy level diagram, with and without impurity. The case without impurity is drawn in a grey color. It can be seen bigger impurity strength has strong shifts of the energy close to the Fermi energy. Fig. 14 (d) shows the density of state (DOS) as a function of energy close to Fermi energy.

In Fig.15 we show the typical and average of the fidelity F , the Anderson integral I_A , and the gap Δ evolution as a function of system size L for two impurity strength $V_0 = 0.1, 10$. In numerical calculation we considered a single impurity randomly located on the chain and averaged over the position. As can be seen the typical and average are the same as expected for the clean model. For impurity strength $V_0 = 0.1$, we found a small power-law decay ($L^{-0.0001}$) for both fidelity and I_A as function of system size. We noticed that fidelity almost touches the I_A as an upper bound limit for all the range of system size shown here. While for the strong impurity case, $V_0 = 10$, fidelity decays much faster with system size ($L^{-0.1}$) and smaller than the I_A for all ranges of system size. However, in both weak and strong impurity, the gap Δ independent of the impurity strength and decays in power-law as L^{-1} .

In Figs.16 and 17 we explore the distributed impurity for both weak and strong cases. For the weak strength $V_0 = 0.1$, we observe fidelity decays in power law with systems size and becomes more slow with increasing the number of sites which impurity is distributed over on. This in agreement with the fidelity behaviour in the metallic phase of the (extended) AA-model reported in the main text. While for strong impurity, see Fig.17, the typical fidelity decreases with M , decaying more fast with a power law of L , the larger M is.

D. Appendix

In this appendix, we present the average numerical results of fidelity and energy spectrum of the AA model reported in the main text. All comparisons has given in place in the main text.

Fig. 18 shows the energy diagram and density of states as function of energy E , as averaged over the random phases ϕ in the Hamiltonian Eq. (3) for $b = 0$ and $\lambda = 2$

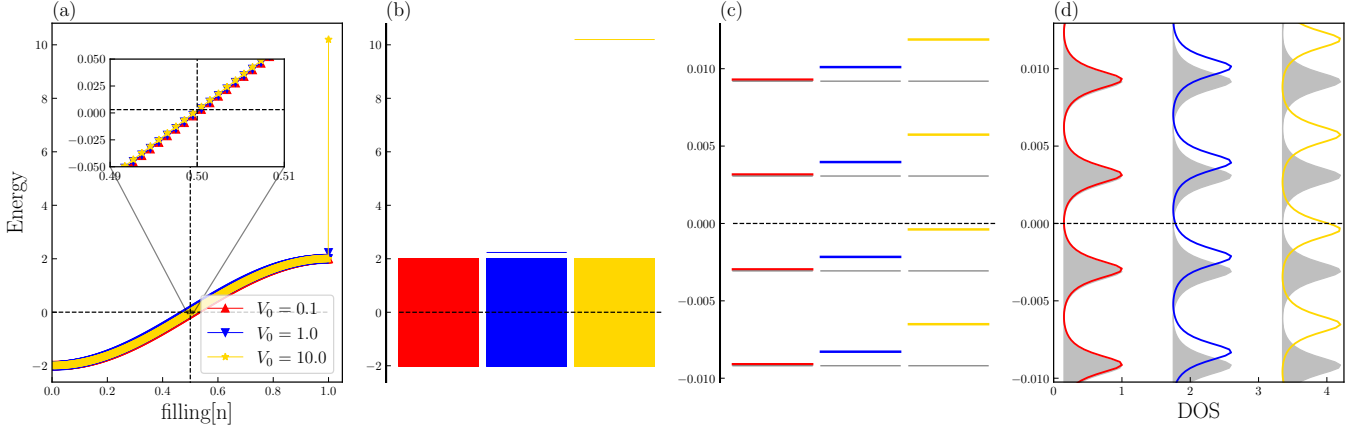


FIG. 14: Energy diagram and density of state for the tight binding model with a single impurity $M = 1$ randomly sitting on the chain.

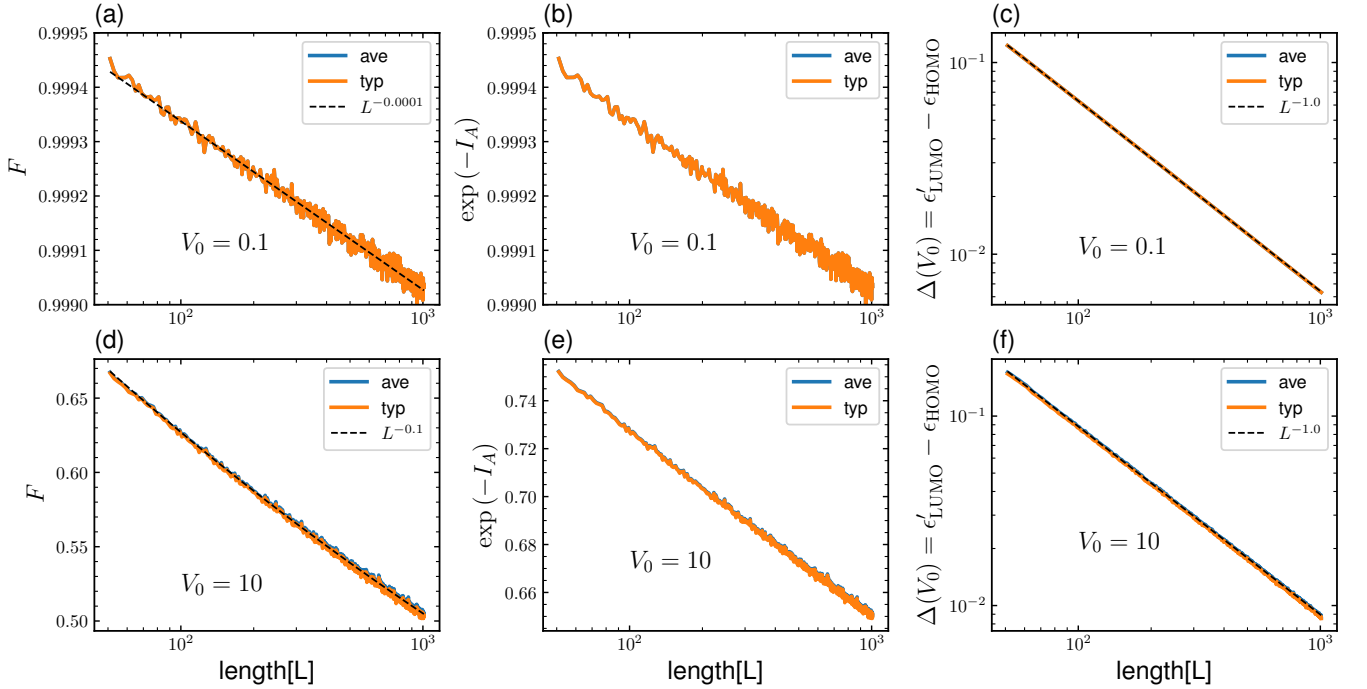


FIG. 15: Average and typical value of the fidelity, Anderson integral and gap evolution as a function of chain length, for the tight-binding model with a single impurity $M = 1$ randomly sites on the chain. Data averaged over 1000 realizations. Black-dashed lines are fitted curves.

of 200 realizations. Fig. 19 and Fig20 show the average fidelity for multi impurity case for two impurity strength

$V_0 = 0.1$ and $V_0 = 20$, respectively.

* j.vahedi@jacobs-university.de

† s.kettemann@jacobs-university.de

¹ P. W. Anderson, Phys. Rev. Lett. 18, 1049 (1967).

² P. Nozieres, C. T. de Dominicis, Phys. Rev. 178, 1097 (1969).

³ B. Altshuler, A. Aronov, JETP 50, 968 (1980),

⁴ J.M. Kinaret, Y.Meir, N.S. Wingreen, P.A. Lee and X.G. Wen, Phys. Rev. B 46, 4681 (1992).

⁵ L. CamposVenuti, H. Saleur, and P. Zanardi, Phys. Rev. B 79, 092405 (2009).

⁶ O. Lychkovskiy, O. Gamayun and V. Cheianov, Phys. Rev. Lett. 119, 200401 (2017).

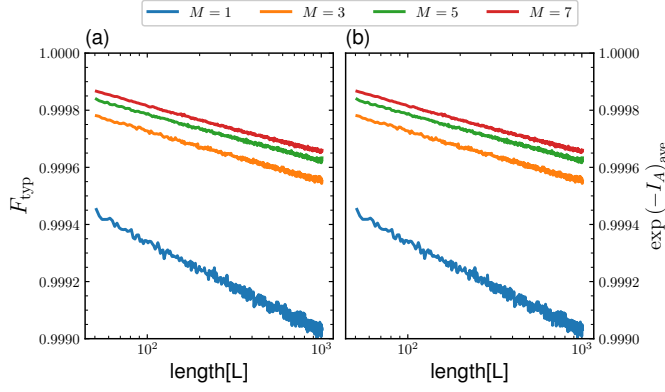


FIG. 16: Typical value of (a) the fidelity and (b) the upper bound $\exp(-I_A)$, for a 1D tight binding model plotted with added impurity Eq. (4) as function of chain length L for different impurity extensions M for fixed impurity strength $V_0 = 0.1$. Data averaged over 1000 realizations.

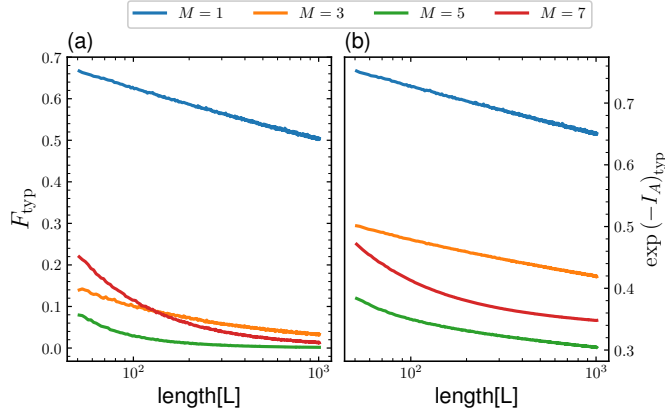


FIG. 17: same as Fig.16, but for impurity strength $V_0 = 10$

- ⁷ M. Knap, A. Shashi, Y. Nishida, A. Imambekov, D. A. Abanin, E. Demler, Phys. Rev. X **2**, 041020 (2012).
⁸ S. Kettemann, Phys. Rev. Lett. **117**, 146602 (2016).
⁹ Y. Gefen, R. Berkovits, I. V. Lerner, B. L. Altshuler Phys. Rev. B **65**, 081106(R), (2002).
¹⁰ V. Khemani, R. Nandkishore, and S. L. Sondhi, Nat. Phys. **11**, 560 (2015).
¹¹ D.-L. Deng, J. H. Pixley, X. Li, and S. Das Sarma, Phys. Rev. B **92**, 220201(R) (2015).
¹² S. Aubry and G. André, Ann. Isr. Phys. Soc. **3**, 133 (1980).
¹³ H. Hiramoto and M. Kohmoto, Int. J. Mod. Phys. B **06**, 281 (1992).

- ¹⁴ S. Ganeshan, J. H. Pixley, and S. Das Sarma Phys. Rev. Lett. **114**, 146601 (2015).
¹⁵ A.-K. Wu, S. Gopalakrishnan and J. H. Pixley, Phys. Rev. B **100**, 165116 (2019).
¹⁶ Fangzhao Alex An, Karmela Padavic, Eric J. Meier, Suraj Hegde, Sriram Ganeshan, J. H. Pixley, Smitha Vishveshwara, and Bryce Gadway Phys. Rev. Lett. **126**, 040603 (2021).
¹⁷ F. Wegner, Z. Phys. B **36**, 209 (1980); H. Aoki, J. Phys. C **16**, L205 (1983); C. Castellani and L. Peliti, J. Phys. A **19**, L991 (1986); M. Schreiber and H. Grubbach, Phys. Rev. Lett. **67**, 607 (1991); M. Janssen, Int. J. Mod. Phys. B **8**, 943 (1994).
¹⁸ J. T. Chalker, Physica A (Amsterdam) **167**, 253 (1990); V. E. Kravtsov and K. A. Muttalib, Phys. Rev. Lett. **79**, 1913 (1997); J. T. Chalker *et al.*, JETP Lett. **64**, 386 (1996); T. Brandes, B. Huckestein, L. Schweitzer, Ann. Phys. (Leipzig) **5**, 633 (1996); V. E. Kravtsov, *ibid.* **8**, 621 (1999); V. E. Kravtsov, A. Ossipov, O. M. Yevtushenko, and E. Cuevas, Phys. Rev. B **82**, 161102 (2010); V. E. Kravtsov, A. Ossipov, O. M. Yevtushenko, J. Phys. A **44**, 305003 (2011).
¹⁹ E. Cuevas and V. E. Kravtsov, Phys. Rev. B **76**, 235119 (2007).
²⁰ M. V. Feigel'man, L. B. Ioffe, V. E. Kravtsov, and E. A. Yuzbashyan, Phys. Rev. Lett. **98**, 027001 (2007); M. V. Feigel'man, L. B. Ioffe, V. E. Kravtsov, E. Cuevas, Annals of Physics **325**, 1368 (2010).
²¹ A. Duthie, S. Roy, and D. E. Logan, Phys. Rev. B **104**, 064201 (2021).
²² E. N. Economou, *Green's Functions in Quantum Physics*, Springer-Verlag, Berlin (1983).
²³ N. Moure, S. Haas, unpublished (2017).
²⁴ K. Slevin, unpublished (2017).
²⁵ S. Kettemann, E. R. Mucciolo, and I. Varga, Phys. Rev. Lett. **103**, 126401 (2009); S. Kettemann, E. R. Mucciolo, I. Varga, K. Slevin, Phys. Rev. B **85**, 115112 (2012).
²⁶ I. V. Lerner Phys. Lett. A **133**, 253 (1988); B. L. Altshuler, V. E. Kravtsov, I. V. Lerner in Mesosc. Phen. in Solids, eds. B. L. Altshuler, P. A. Lee, R. A. Webb, North Holland, 449 (1991).
²⁷ A. D. Mirlin, Phys. Rep. **326**, 259 (2000).
²⁸ L. J. Vasquez, A. Rodriguez, and R. A. Romer, Phys. Rev. B **78**, 195106 (2008).
²⁹ F. Evers and A. D. Mirlin, Rev. Mod. Phys. **80**, 1355 (2008).
³⁰ B.-B. Wei, Phys. Rev. A **99**, 042117 (2019).
³¹ M. Thakurathi *et al* Phys. Rev. B **86**, 245424 (2012).
³² T. Cookmeyer *et al* Phys. Rev. B **101**, 174203 (2020).
³³ M. Amini, V. E. Kravtsov, and M. Müller, New J. Phys. **16**, 015022 (2014); I. S. Burmistrov, I. V. Gornyi, and A. D. Mirlin, Phys. Rev. Lett. **111**, 066601 (2013); Y. Harashima and K. Slevin, Phys. Rev. B **89**, 205108 (2014).

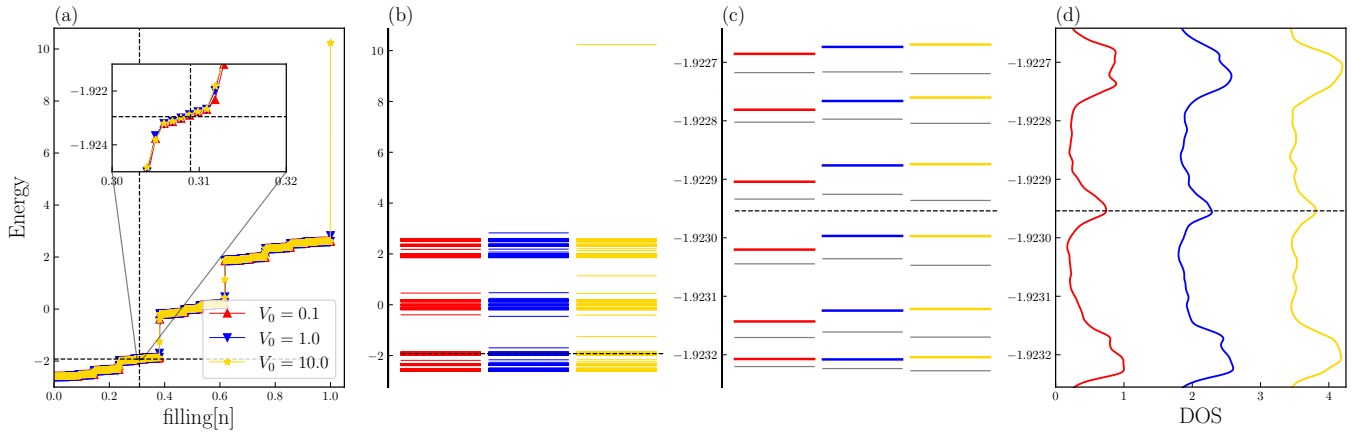


FIG. 18: Same as Fig 2 but with averaging over 200 realizations.

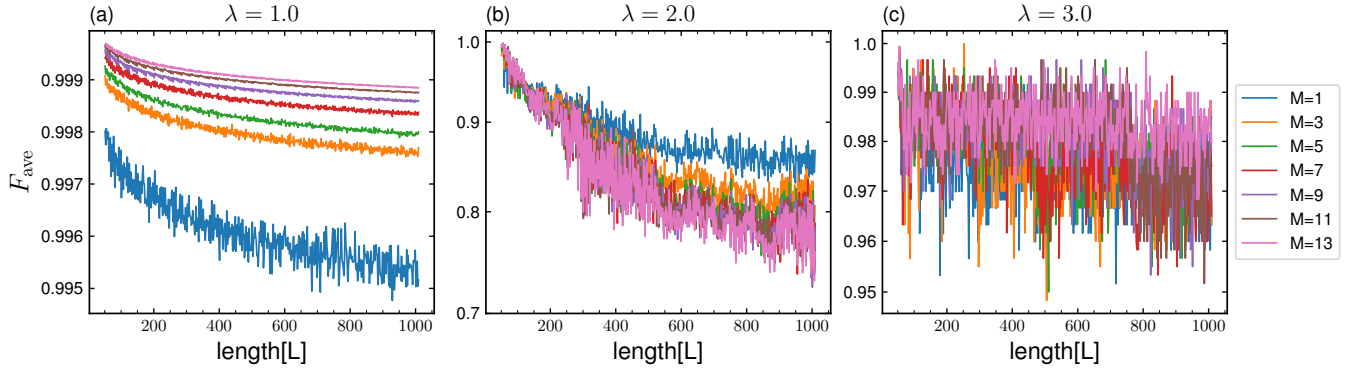


FIG. 19: Same as Fig.7 for a weak impurity but for the average value of fidelity $\langle F \rangle$, and data sampled over 1000 realizations.

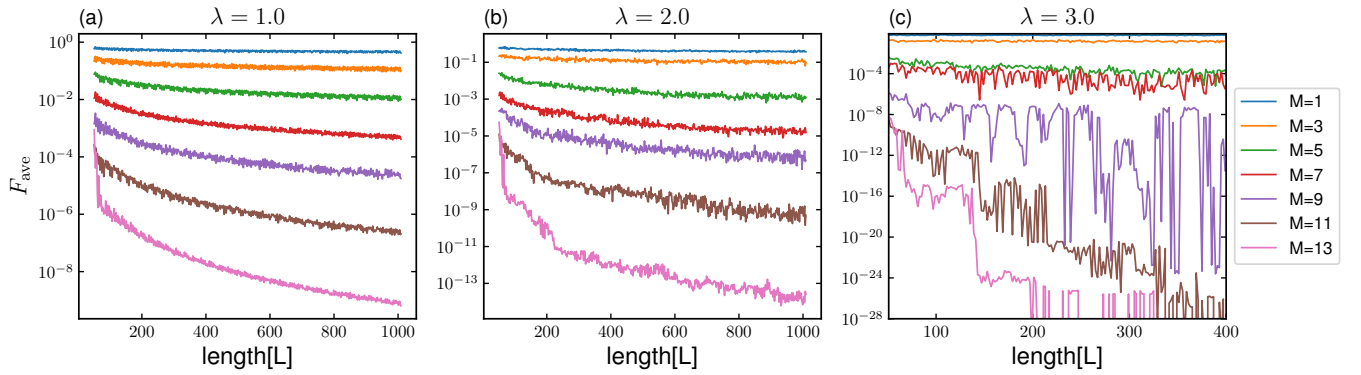


FIG. 20: Same as Fig.10 but for the average value of fidelity $\langle F \rangle$ with a strong impurity, and data sampled over 1000 realizations.